6

Multiscale Routes to Supply Nutrients Through the Kuroshio Nutrient Stream

Takeyoshi Nagai[1], Sophie Clayton[2], and Yusuke Uchiyama[3]

ABSTRACT

In this study, the role of the Kuroshio as a nutrient conduit is discussed using results from recent in-situ observations and numerical simulations. It is shown that nutrient concentrations in the Kuroshio are elevated compared to those in ambient waters of the same density, similar to the Gulf Stream. The source of the Kuroshio nutrient stream appears to be the tropical western North Pacific on the south side of the North Equatorial Current. Along its path, widespread vigorous subsurface turbulence with an average eddy diffusivity of $O(10^{-4}$ $m^2s^{-1})$ associated with near-inertial waves is observed in the Tokara Strait, where the upstream Kuroshio flows over shallow topography and seamounts. In the Kuroshio Extension, subinertial shear forms thermohaline interleaving structures, which induce double-diffusive convection with an average subsurface thermal diffusivity of $O(10^{-3}$ $m^2s^{-1})$. These very strong diapycnal mixing processes appear to be important for the upward nutrient supply. An eddy-induced nitrate flux is directed mostly downward and offshore, removing nutrients in the region between the Kuroshio and the Japanese coast off Honshu Island. In contrast, on the north side of the Kuroshio Extension, where warm streamers and warm core eddies emanate from the Kuroshio Extension, the eddy-induced nitrate flux is upward and northward.

6.1. INTRODUCTION

One of the most compelling scientific puzzles for many oceanographers, including those in fisheries, has been to understand why many pelagic fish populations in the western North Pacific utilize the Kuroshio region for spawning, fixing the destinies of their juveniles to be carried along the Kuroshio, a warm nutrient-poor western boundary current of the North Pacific. The key to unravelling the mystery of the "Kuroshio paradox" (Saito, Chapter 1 this book), which we introduce in this chapter, may lie under the surface of the Kuroshio waters.

[1] *Department of Ocean Sciences, Tokyo University of Marine Science and Technology, Tokyo, Japan*

[2] *Ocean, Earth & Atmospheric Sciences Department, Old Dominion University, Norfolk, VA, USA*

[3] *Department of Civil Engineering, Kobe University, Hyougo, Japan*

At the ocean surface, satellite remote sensing of phytoplankton pigment concentrations clearly indicates that the western North Pacific subtropical region is basically an ocean desert, sustaining very low concentrations of chlorophyll *a* (Figure 6.1). The Kuroshio and the Kuroshio Extension flow along the western and northern edges, respectively, of this ocean desert, which separates the high chlorophyll waters of Kuroshio–Oyashio confluence to the north and the region between the Kuroshio and the Japanese archipelago. However, taking a closer look at the regions along the Kuroshio Extension in the winter and spring seasons, in which the deepening of the surface mixed layer in winter mixes the subsurface nutrients, followed by restratification in spring, the chlorophyll *a* concentrations are substantially elevated along the northern edge of the Kuroshio Extension (35°N, 145–180°E). One explanation for this increase is that the chlorophyll *a* is transported from the nutrient-rich Oyashio water, but it is not clear why chlorophyll *a* concentrations

Kuroshio Current: Physical, Biogeochemical and Ecosystem Dynamics, Geophysical Monograph 243, First Edition.
Edited by Takeyoshi Nagai, Hiroaki Saito, Koji Suzuki, and Motomitsu Takahashi.

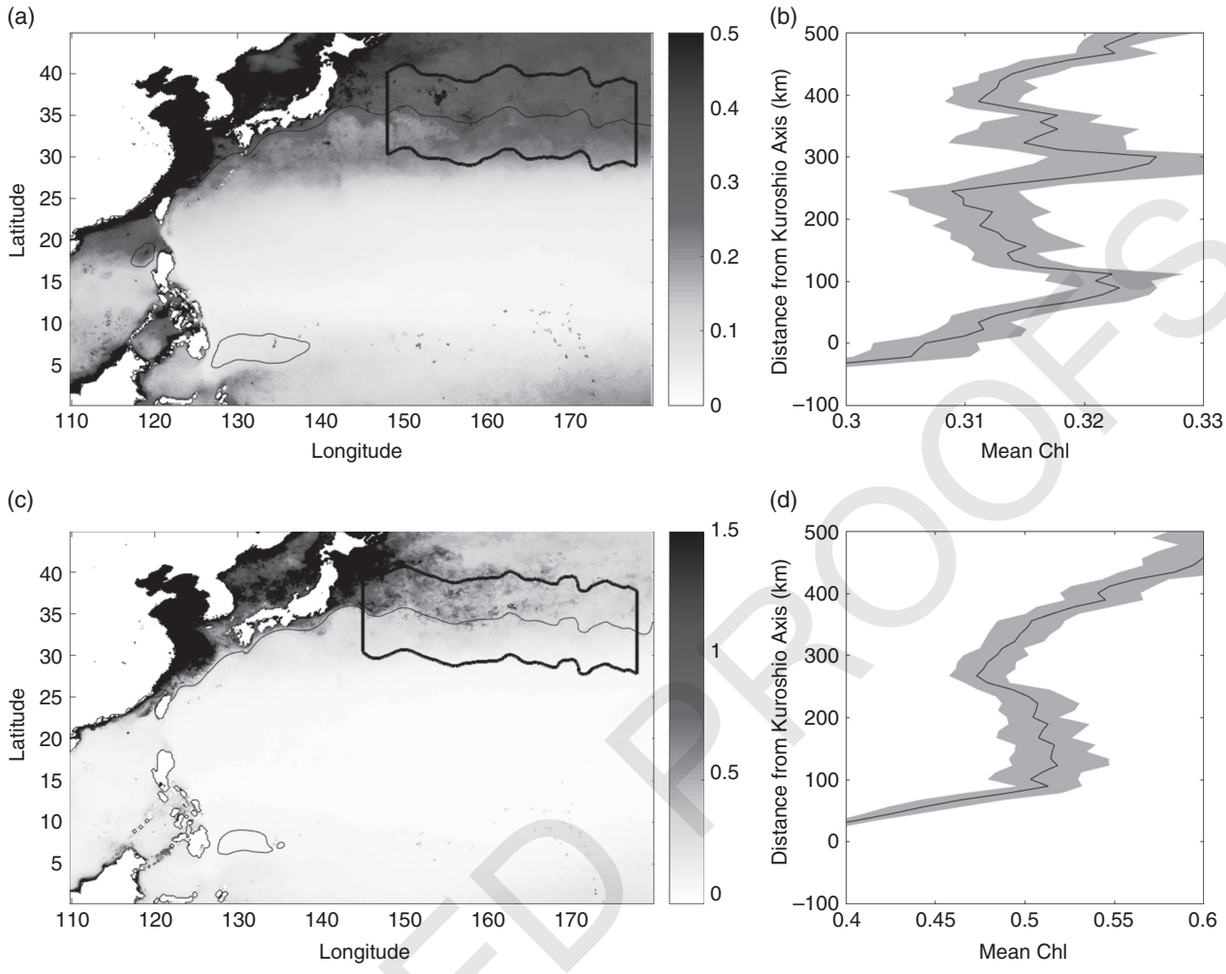

Figure 6.1 MODIS satellite seasonal climatological sea surface chlorophyll *a* concentrations in the western North Pacific subtropical region (mg m^{-3}) for winter (a) and spring (c). Average chlorophyll *a* within the regions bounded by thick black curves in (a) and (c) are shown for winter (b) and spring (d), respectively, as a function of distance from the Kuroshio Axis (positive northward), defined at the AVISO climatological sea surface height of 0.9 m, which is indicated by black contours in (a) and (c). Shading in (b) and (d) is 95% confidence interval. Note that, in (b) and (d), the mean chlorophyll concentrations mostly on the north side of the Kuroshio Extension are shown.

are higher at the northern edge of the Kuroshio Extension than that in adjacent regions further north, closer to the Oyashio. Another potential explanation for the high chlorophyll *a* associated with the northern flank of the front is advection of high chlorophyll water from the Japanese coast by the Kuroshio, and/or lateral transport of nutrients from coastal waters. These lateral advections should certainly contribute to the elevated chlorophyll *a* concentrations observed along the Kuroshio Extension.

However, it is not clear why the coastal waters have higher chlorophyll *a* concentrations over such a fairly wide area despite the narrow continental margin along the Japanese coast, or how the nutrients are supplied to maintain relatively high phytoplankton concentrations near the coast. This might be explained by an eddy-induced nutrient upward flux (McGuillicuddy et al., 2003, Oschiles et al., 2003) caused by mesoscale eddies emanating from the Kuroshio and the Kuroshio Extension. However, assuming a zonal front with abundant nutrients on the northern side of the front, the southward horizontal shift of the preexisting domed nutrient-rich cold water in a cyclonic eddy may experience average subduction due to stretching of the water column (Levy et al., 2001) and may not be effective in causing an increase in primary production. The nonlinear mesoscale eddies generated through baroclinic instability advects the shallow pycnocline from the northern side to the southern side of the front, and the deep pycnocline from the southern to the northern side of the front, which acts to restratify the front. Also, as these mesoscale eddies are more frequently found in the

Kuroshio–Oyashio confluence region, this mechanism does not explain the elevated chlorophyll *a* concentrations observed along the Kuroshio Extension. In addition, recent numerical studies on the role of mesoscale eddies in the coastal upwelling region in the California Current System showed that the mesoscale eddies tend to subduct the upwelled nutrients, suppressing primary production (Gruber et al., 2011; Nagai et al., 2015c). Assuming abundant nutrients on the cold and dense northern side of the Kuroshio Extension, which is a similar situation to that in the coastal upwelling regions where abundant nutrients are in cold and dense upwelled water near the coast, we speculate that the eddy-induced circulations also tend to subduct the nutrients in the Kuroshio region (Lee & Williams, 2000). The role of mesoscale eddies in nutrient transport and primary production in the Kuroshio and the Kuroshio Extension regions has thus been elusive.

On the other hand, previous studies of the Gulf Stream, a western boundary current in the North Atlantic, found that it is a nutrient stream in its subsurface layer, which transports a large amount of nutrients from the south to subpolar regions downstream (Pelegrí & Csanady, 1991; Pelegrí et al., 1996, Chapter 3 this book). In addition, the nutrient concentrations are elevated along the stream, compared to those found in the ambient water of the same density (Pelegrí et al., 1996). Further analyses using a numerical model have suggested that nutrients carried by the Gulf nutrient stream might originate in the tropical ocean, and even farther south in the Southern Ocean (Williams et al., 2006, 2011). It has also been shown that the ultimate supply of nutrients to the euphotic zone through this Gulf nutrient stream can be achieved by induction as the stream encounters a deeper mixed layer toward the north, which enables the nutrients to be carried laterally through the mixed layer base to mix with the sunlit surface layers (Williams et al., 2006). In the North Pacific, the observations off southeast Taiwan by Chen et al. (1995) and those in the Okinawa Trough (Chen, 1996; Guo et al., 2012) found that the subsurface layers of the Kuroshio also transport a large amount of nutrients to the north, and that nutrient concentrations increase in the downstream direction, probably supplied by recirculation gyres (Guo et al., 2013). Accordingly, the subsurface Kuroshio nutrient stream appears to be a conduit for nutrient enrichment in the region between the Kuroshio and the Japanese coast, and the Kuroshio Extension region. This is supported by a number of observational studies on the Kuroshio-influenced coastal seas, which have reported that bottom intrusions of cold saline nutrient-rich water into the Bungo Channel, Japan, are accompanied by Kuroshio water intrusions (Kaneda et al., 2002; Arai, 2005; Kuroda, Chapter 8 this book). Because the Kuroshio is known as an oligotrophic nutrient-poor warm current, these findings are somewhat counterintuitive, but consistent with the idea that the Kuroshio acts as a subsurface nutrient stream.

Although the Kuroshio is considered a nutrient stream similar to the Gulf Stream, it is not clear whether the nutrient concentrations along constant density surfaces are elevated within the Kuroshio nutrient stream, as has been found in the Gulf Stream. The mechanisms which form and maintain the elevated nutrient concentrations within these nutrient streams are not well understood. Mesoscale along-isopycnal stirring tends to homogenize any tracer anomalies formed along density surfaces. The timescale at which mesoscale stirring diffuses the along-isopycnal nutrient anomaly can be estimated using a ratio of squared width of the anomaly δx^2 to the along-isopycnal diffusivity K_e caused by mesoscale eddies, $\delta x^2/K_e$. With the previously reported K_e of $O(10^4\ m^2s^{-1})$ (Wolfram et al., 2015) in the western boundary current regions, and assuming 100 km for the widthδx of the nutrient stream, the timescale can be estimated as a few tens of days, which is much shorter than the advection timescale along the Kuroshio nutrient stream ~100 days (see section 6.3). Accordingly, the along-isopycnal nutrient anomaly, which persists even in its downstream regions, implies that the across-density surface, i.e., diapycnal flux, should be important in generating and/or maintaining the observed elevated nutrient concentrations within the nutrient streams. A previous study speculated that diapycnal mixing caused by vertical shear of the Gulf Stream generates elevated nutrient concentrations along the stream (Pelegrí et al., 1996). However, coarse lateral resolution microstructure measurements made during the 1970s and 1980s did not show any enhanced turbulence at the Gulf Stream front. In contrast, recent microstructure surveys have observed relatively large turbulent dissipation rates in the thermocline of the Gulf Stream (Inoue et al., 2010) and the Kuroshio, which can be attributed to propagating near-inertial internal waves (Nagai et al., 2009, 2012, 2015a; Kaneko et al., 2012, 2013). While a simple induction process was proposed and evaluated as the ultimate supply process of the Gulf nutrient stream in subpolar regions, many recent studies have shown that submesoscale processes in the upper layers of the fronts and eddies play a role in vertical nutrient supply (Mahadevan & Archer, 2000), the onset of the phytoplankton blooms (Mahadevan et al., 2012), and carbon export (Omand et al., 2015). Because the supply regions of the Kuroshio nutrient stream, i.e., the Kuroshio Extension front and Kuroshio–Oyashio confluence region, are full of these rich submesoscale streamers and filaments, it is likely that these submesoscale processes play a very important role for nutrient supply, in addition to the simple induction process.

In this study, we analyze climatological nitrate data and historical in situ observation data to show for the first

time that nutrient concentrations are indeed elevated along density surfaces within the Kuroshio nutrient stream. Then, using the new results from a numerical simulation, we investigate the source of the nutrients in the Kuroshio nutrient stream. Based on our previous results, the role of eddies in nutrient transport is summarized. Finally, a series of previous in situ observations of the authors showing the important diapycnal mixing processes for nutrient diffusion and supply in the upstream and downstream Kuroshio is discussed.

6.2. ELEVATED NUTRIENTS ALONG THE KUROSHIO NUTRIENT STREAM

A previous study focusing on nitrate concentrations across a repeated section, the PN line in the upstream Kuroshio, in the Okinawa Trough, showed that the Kuroshio transports a large amount of nitrate at a rate of 170.8 k mol N s^{-1} (Guo et al., 2012). This study focused on advective nitrate transport driven by a combination of a strong and deep Kuroshio current and increasing nitrate concentrations with depth, resulting in a subsurface nitrate conduit. However, it has yet to be determined whether the nutrient concentrations along the Kuroshio nutrient stream are elevated, as they are in the Gulf Stream. To address this, the annual mean nitrate concentration from World Ocean Atlas 2013 data (Garcia et al., 2014) is sliced on the density surface at $\sigma_\theta = 25\,kg\,m^{-3}$ (Figure 6.2). The concentration is clearly elevated along the western boundary of the North Pacific where the Kuroshio flows from the southwest to the northeast (Figure 6.2a). The relatively high nitrate concentrations found along the Kuroshio and in the adjacent waters between the Kuroshio and Japanese coast may explain why high chlorophyll *a* concentrations are seen in these regions. The depth of the density layer of $\sigma_\theta = 25\,kg\,m^{-3}$ becomes shallower toward the downstream of the Kuroshio nutrient stream (Figure 6.2b). During the winter, the climatological mean density suggests that the density layer of $\sigma_\theta = 25\,kg\,m^{-3}$ outcrops in regions from 30–32°N to the north, suggesting that nitrate on this density layer is entrained into the surface mixed layer where it fuels phytoplankton growth (Figure 6.2c).

To investigate this elevated nitrate on a regional scale, in situ nitrate data from 1997 to 2015 along the PN line (Guo et al., 2012) were bin averaged as a function of σ_θ and the distance from the Kuroshio axis, defined here as the location of the maximum surface velocity magnitude. The bin-averaged nitrate concentration shows relatively high values along the same density surface near the Kuroshio axis (Figure 6.3), consistent with that seen in the World Ocean Atlas (Figure 6.2) and with the Gulf nutrient stream (Pelegrí et al., 1996). Downstream, the same bin-averaged nitrate data obtained in October 2009 across the Kuroshio Extension front (Nagai et al., 2012; Clayton et al., 2014) also show elevated nitrate concentrations in the Kuroshio Extension front (Figure 6.4) (Nagai & Clayton, 2017). In this case, the elevated nitrate is seen in relatively less dense water ($\sigma_\theta = 23.5$–$25\,kg\,m^{-3}$) compared to that found in the PN Line ($\sigma_\theta = 25.5$–$24.5\,kg\,m^{-3}$; Figure 6.3). This suggests that there are nutrient diapycnal transports caused by microscale mixing processes (see section 6.5) that occur between upstream regions in Okinawa Trough and the downstream Kuroshio Extension region. The high nitrate concentrations in the $\sigma_\theta = 26\,kg\,m^{-3}$ density layer are also seen on the northern side of the Kuroshio Extension ($\sigma_\theta = 26\,kg\,m^{-3}$ 0-60 km in Figure 6.4), which is considered to be a deeper part of the nutrient stream, because this density layer has previously been reported as the core of the Kuroshio nutrient stream in the upstream PN Line (Guo et al., 2012).

6.3. SOURCE OF THE NUTRIENTS IN THE KUROSHIO NUTRIENT STREAM

The World Ocean Atlas data show high nitrate concentrations following the path of the Kuroshio density surface, upstream and at its origin, Luzon Strait and off the Philippine islands (Figure 6.2a). Because water movements in the ocean interior tend to follow density surfaces, the likely source regions for the elevated nitrate along the Kuroshio might be the southern edge of the subtropical gyre, which could be connected to the tropical western North Pacific, as well as the South China Sea, given a clockwise upper layer circulation of the North Pacific subtropical gyre. It is suggested that the Kuroshio nutrient stream transports nitrate from these southern regions to the Kuroshio Extension and the Kuroshio–Oyashio confluence region.

To identify the source regions for the elevated nitrate, the Regional Oceanic Modeling System (ROMS) coupled with a simple nitrogen-based, nitrate-ammonium-phytoplankton-zooplankton large and small detritus N_2PZD_2 model (Gruber et al., 2006; Nagai & Clayton, 2017) was used to simulate the Kuroshio nutrient stream. The model was eddy permitting with a slightly higher lateral resolution of ~10 km in the Kuroshio region, with 64 vertical levels, and forced with monthly Comprehensive Ocean Atmosphere Data Set (COADS) (da Silva et al., 1994) climatology for the first five years; for the following 16 years the model was forced with six-hourly NCEP CFS Reanalysis from 1980 to 1995 (NCEP, 2015), with lateral boundary conditions set from World Ocean Atlas (Garcia et al., 2014) at the open boundaries. The simulation was for 21 years in total, and the output from the final year was used in this study.

The model successfully reproduces the satellite-observed sea surface height, chlorophyll *a* concentrations, and the

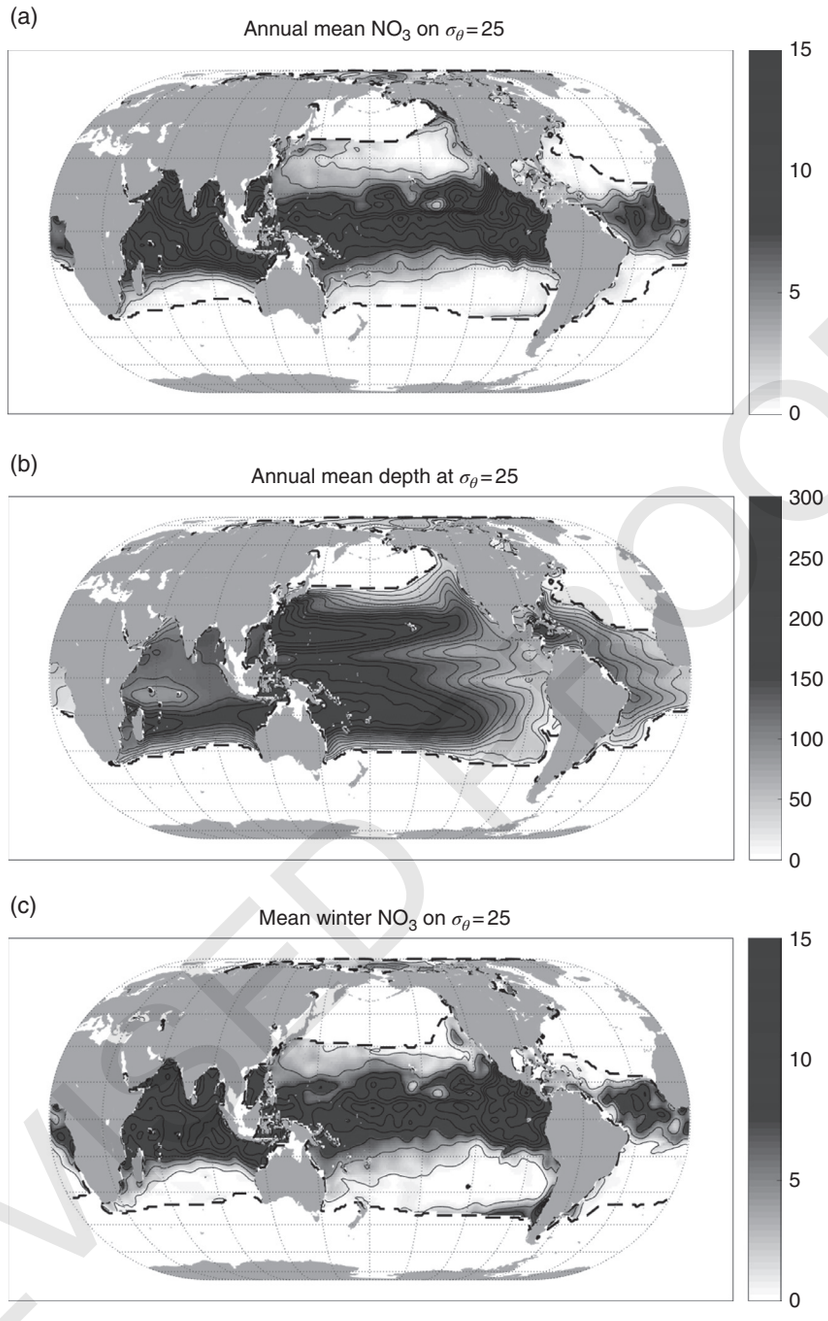

Figure 6.2 World Ocean Atlas 2013 (Garcia et al., 2014) for (a) annual mean nitrate concentrations (m mole m^{-3}) sliced at $\sigma_\theta = 25\,kg\,m^{-3}$, (b) annual mean depth of the density layer (m), and (c) nitrate concentrations (m mole m^{-3}) sliced at $\sigma_\theta = 25\,kg\,m^{-3}$ during winter. Dashed contour represents outcropping positions. (*See insert for color representation of this figure*.)

nitrate in situ data across the Kuroshio Front (Nagai & Clayton, 2017). Similar to the result shown in Figure 6.2, the modelled nitrate concentration on 30 June sliced at the density surface of $\sigma_\theta = 25\,kg\,m^{-3}$ shows that nitrate concentrations are elevated along the western boundary of the North Pacific following the Kuroshio path (Figure 6.5a) and are comparable to concentrations found in the World Ocean Atlas (Figure 6.2a). The meridional nitrate gradient at around 15°N in the western to the central North Pacific is also reproduced well. On 15 March, the density layer of $\sigma_\theta = 25\,kg\,m^{-3}$ outcrops at around 30°N, similar to the World Ocean Atlas, suggesting that the modelled

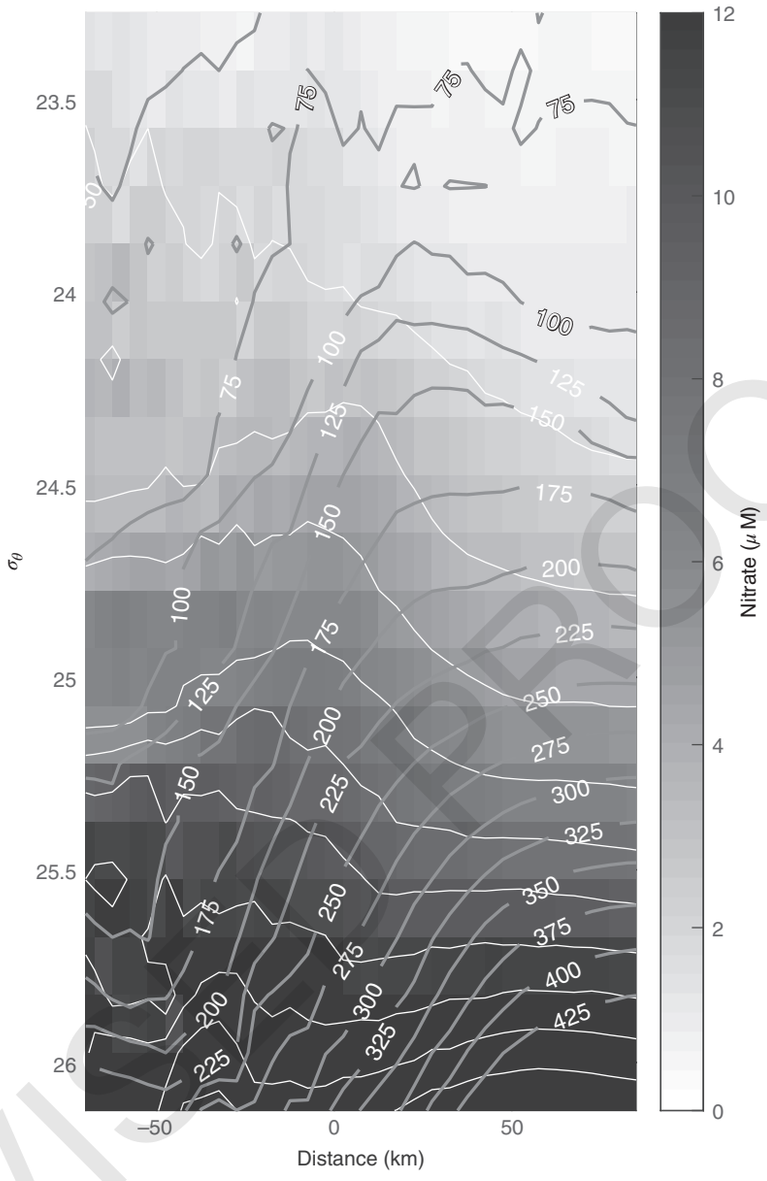

Figure 6.3 Bin-averaged nitrate concentration (m mole m^{-3}) obtained along the PN Line in the Okinawa Trough during 1997 through 2015 as a function of σ_θ and the distance from the Kuroshio axis defined at the maximum surface velocity is shown as shading. The gray contours show depth (m).

nitrate transported to the Kuroshio Extension is also entrained into the surface mixed layer during winter time.

To investigate the source of the nitrate transported along the path of the Kuroshio, a passive tracer initialized with the same distribution as the modeled nitrate on 30 December of the previous year, but filled with zero values from 17–18°N, south of Luzon Strait to the north, and from 120°E to the west, was released on 1 January. After 15 days, the tracer on the $\sigma_\theta = 25\,kg\,m^{-3}$ density layer flows across Luzon Strait and approaches Taiwan (Figure 6.6a). A large fraction of the tracer passes through the East China Sea and reaches south of Honshu Island after 225 days (7–8 months; Figure 6.6b). The results on the $\sigma_\theta = 25\,kg\,m^{-3}$ layer show that the Kuroshio can transport the tracer from the Philippine islands to the Kuroshio Extension region in roughly one year (345 days) (Figure 6.6c). The same tracer experiment was repeated for nitrate originating only from the South China Sea with the initial tracer released from 120°E to the west. The fraction of the South China Sea origin tracer in the

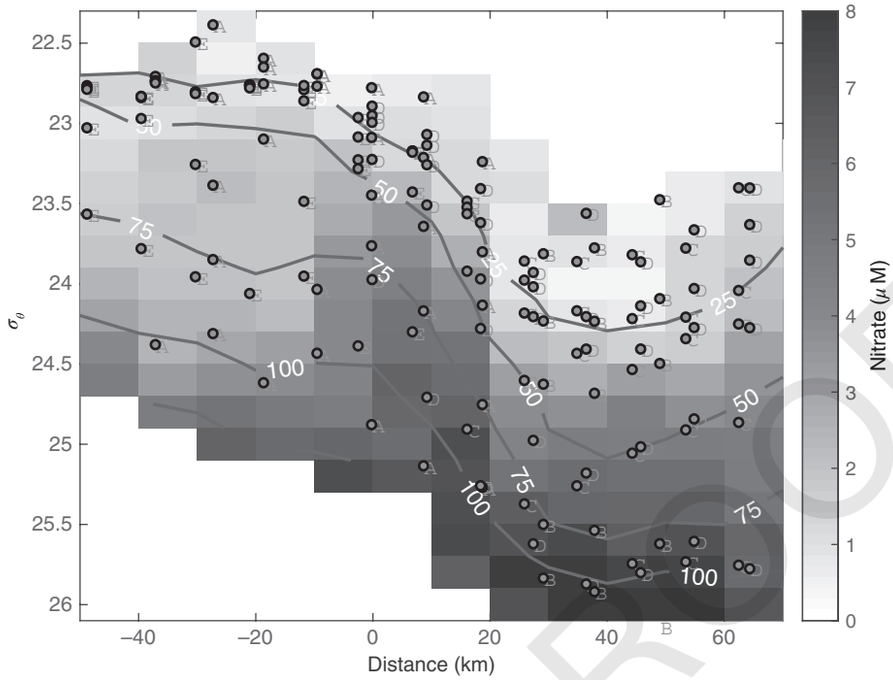

Figure 6.4 The same figure as Figure 6.3 but for nitrate (m mole m^{-3}) measured during October 2009 in the Kuroshio Extension. The gray contours show depth (m), and the alphabet characters A–E represents the origins in the five north–south transects shown in Figure 6.15a.

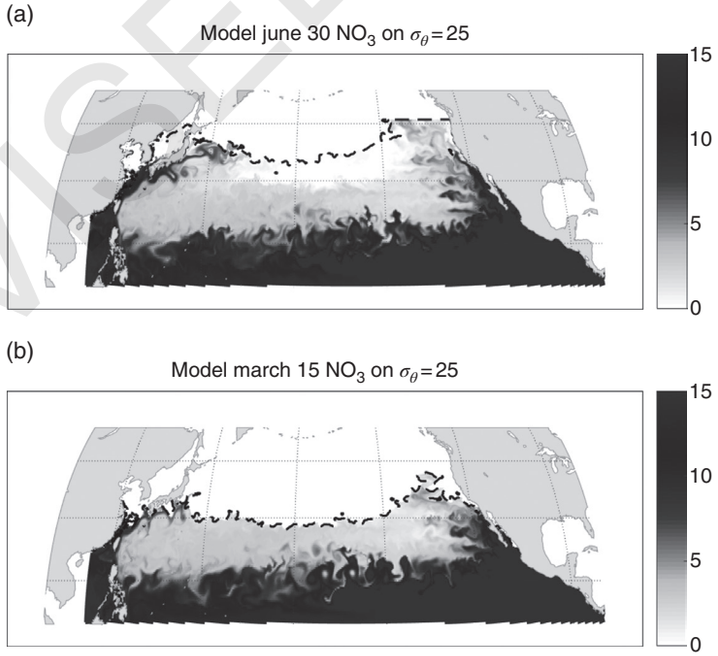

Figure 6.5 Modeled nitrate concentrations (m mole m^{-3}) on the density surface at $\sigma_\theta = 25\,kg\,m^{-3}$ for (a) 30 June and (b) 15 March. The dashed contours show the outcropping positions.

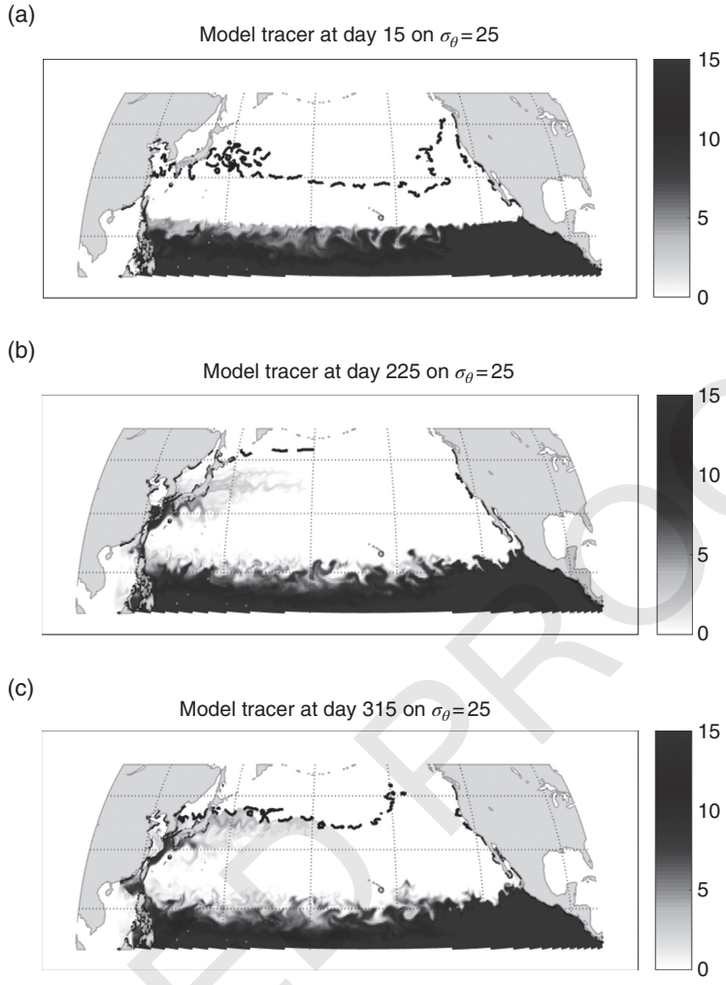

Figure 6.6 Passive tracer distributions released from the tropical regions of North Pacific at (a) 15 days, (b) 225 days, and (c) 345 days after the release. The passive tracer initial condition is taken from modeled nitrate on 1 January (m mole m^{-3}). The dashed contours show the outcropping positions.

downstream Kuroshio regions after 345 days is found to be only 1–3% relative to the contribution from the southwestern North Pacific. Some of the tracer released from the South China Sea enters the East China Sea (not shown). Previous studies have pointed out that the Kuroshio water intrudes significantly into the South China Sea (Nan et al., 2015) and our results suggest that once the nutrients in the Kuroshio nutrient stream enter the South China Sea, most of them are subsequently not transported to the downstream Kuroshio regions.

6.4. EDDY-INDUCED NITRATE FLUX IN THE KUROSHIO AND THE KUROSHIO EXTENSION

As mentioned in the introduction, the role of mesoscale eddies in transporting nutrients in the Kuroshio region is not well understood. To quantify the eddy nitrate flux, a ROMS simulation was conducted with ~3-km resolution in the Kuroshio region (Uchiyama et al., 2017). The eddy nitrate flux was then computed by Reynolds decomposition as follows:

$$F_H = \overline{Nv} = \bar{N}\,\bar{v} + \overline{N'v'}$$
$$F_v = \overline{Nw} = \bar{N}\bar{w} + \overline{N'w'} \tag{6.1}$$

where the last terms on the right-hand side of the equations are eddy-induced nitrate flux along the meridional $\overline{N'v'}$ and vertical directions $\overline{N'w'}$, respectively; the overbar represents a low-pass filter at 90 days; the prime is a fluctuation from the low-pass filter; N is nitrate; and v and w are meridional and vertical velocities, respectively. The fluctuations decomposed by equation (6.1) include meso and submesoscale variabilities. The resultant eddy vertical flux averaged within the upper 200 m

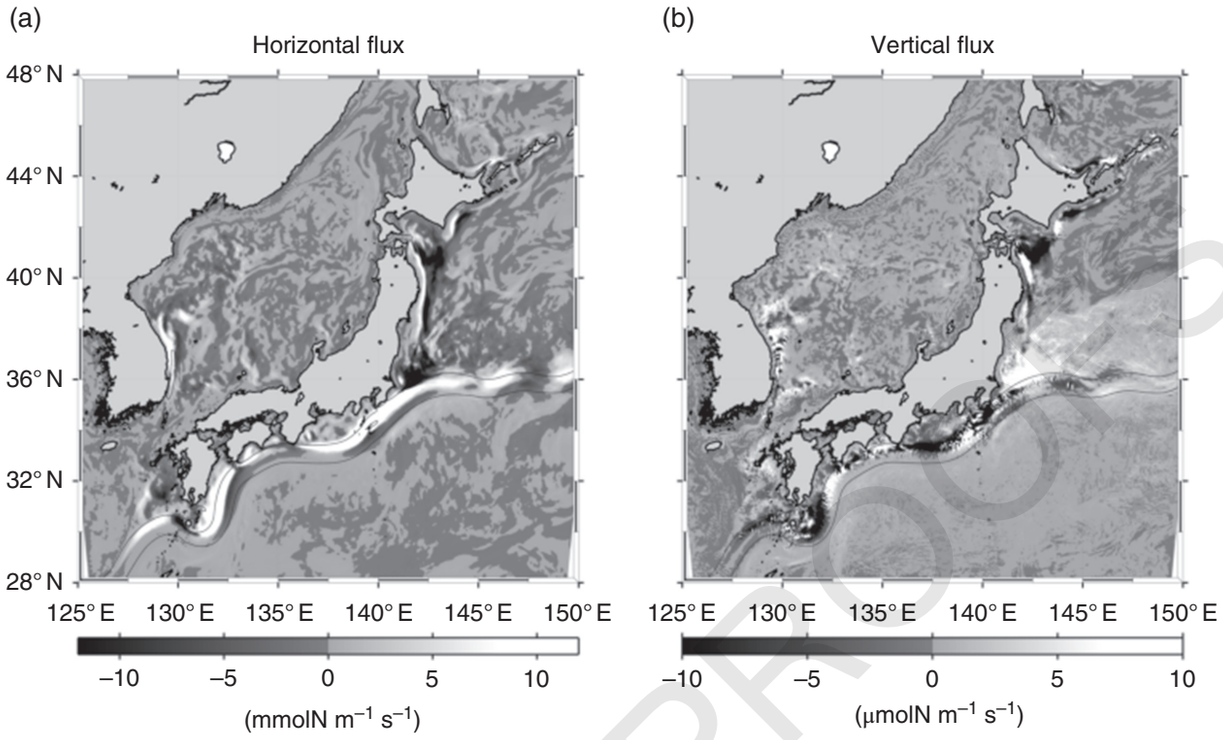

Figure 6.7 Eddy-induced nitrate flux (a) along the meridional direction and (b) along the vertical direction averaged within the upper 200 m depth. White (positive) represents southward and upward directions in (a) and (b), respectively, and vice versa for black (negative). The black curves indicate the approximate Kuroshio Current.

shows dominant downward flux, especially in the meander troughs of the Kuroshio south of Honshu Island (Figure 6.7b). In this region, the eddy meridional flux points mostly southward (Figure 6.7a), suggesting that the eddies and filaments near the Kuroshio off Honshu Island tend mostly to remove abundant nitrate in the regions between the Kuroshio and southern coast to the subsurface layers in the offshore regions (Figure 6.8a and 6.8b). This result is similar to that obtained by the same analyses conducted on the California Current System (Gruber et al. 2011; Nagai et al. 2015c) and is consistent with the results of Lee & Williams (2000), in which the nutrient concentration was set on the north side of the zonal front. Because along-isopycnal meridional gradient of nitrate is mostly positive between the coast of Honshu Island and the Kuroshio (Figure 6.5a), with a large amount of the nitrate transported by the subsurface Kuroshio nutrient stream, eddy-induced circulations, which tend to restratify the front, result in southward (offshoreward) and downward eddy-induced nitrate fluxes (Figure 6.7, 6.8a and 6.8b).

In contrast, the large upward and northward eddy-induced nitrate fluxes are seen north of the first meander crest of the Kuroshio Extension, with southward and downward eddy fluxes produced on the south side (Figure 6.7, 6.8c and 6.8d). This tendency continues toward east along the Kuroshio Extension (Figure 6.7). As seen in the modeled nitrate concentrations (Figure 6.5) and in the World Ocean Atlas (Figure 6.2), on the $\sigma_\theta = 25\,\mathrm{kg\,m^{-3}}$ density surface, and the bin-averaged nitrate as a function of distance from the Kuroshio Extension axis and σ_θ (Figure 6.4), the along-isopycnal nitrate increases and then decreases with latitude across the Kuroshio Extension. The positive along-isopycnal meridional gradient of nitrate on the south side of the Kuroshio Extension and the negative gradient on the north side correspond to the cases of high nitrate concentration on the north and on the south of the zonal front, respectively (Lee & Williams, 2000). In the former case, the eddy-induced flux is southward and downward. On the contrary, the eddy-induced flux in the latter case is directed to northward and upward, consistent with the model results (Figure 6.7, 6.8c and 6.8d). It should be noted that both fluxes, directed northward and upward on the north, and southward and downward on the south side of the Kuroshio Extension nutrient stream act to homogenize the positive along-isopycnal nitrate anomaly advected by the Kuroshio nutrient stream.

On the north side of the Kuroshio Extension nutrient stream, filaments of warm water, i.e., warm streamers, are frequently generated and transport heat to warm core eddies propagating to the north of the Kuroshio Extension

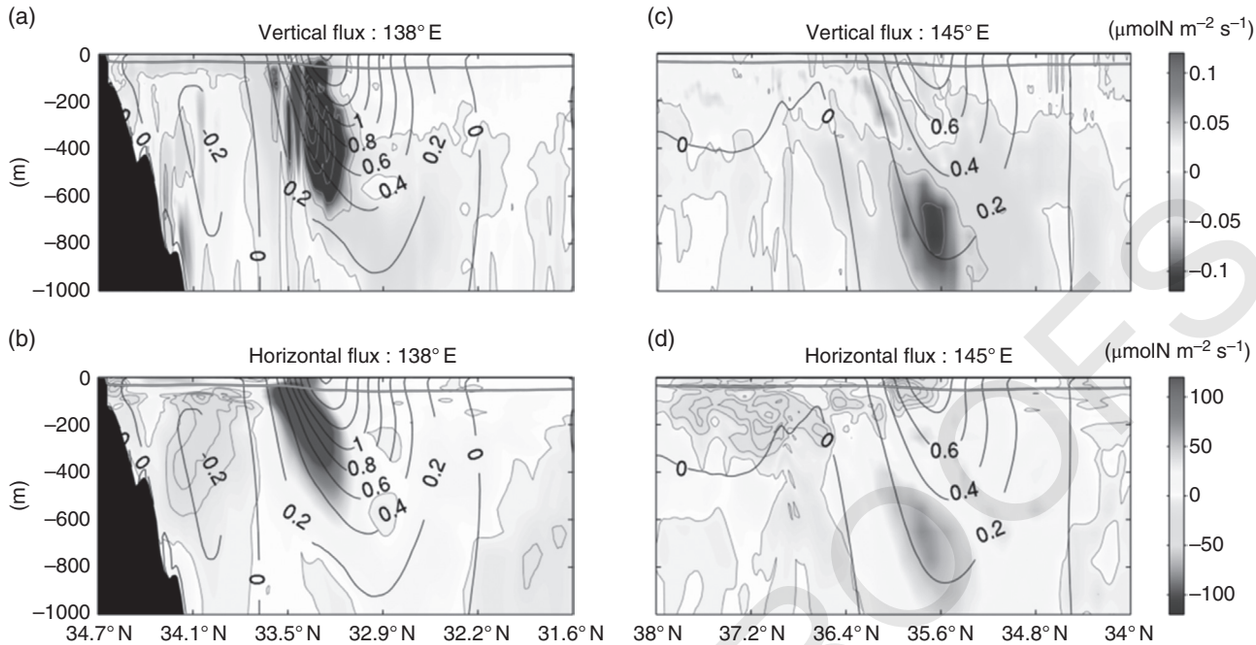

Figure 6.8 Vertical sections of eddy-induced nitrate flux along (a–b) 138°E and (c–d) 145°E for (a and c) vertical and for (b and d) meridional flux. Blue with thin broken contours represents northward and downward directions. Thick solid contours show mean current velocity. Magenta horizontal curves indicate the mixed layer depths. (*See electronic version for color representation of this figure*.)

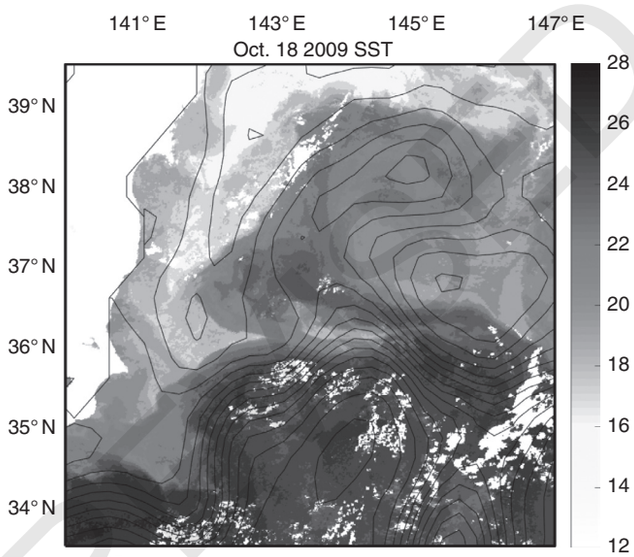

Figure 6.9 A warm filament or warm streamer observed in the satellite sea surface temperature data during the October 2009 cruise by the R/V Natsuushima. The black contour represents AVISO sea surface height averaged during the observation period.

(Yasuda, 1995) (Figure 6.9). These thin filaments are induced by large mesoscale deformations. For cold streamers, the frontogenetic deformation at the two fronts bounding the cold filament produces pronounced downwelling (McWilliams et al., 2009). On the other hand, the frontogenetic deformation at the two fronts bounding a warm streamer generates upwelling in the warm streamers (Figure 6.10; Klein & Lapeyre, 2006). We speculate that the northward and upward eddy-induced nitrate flux shown in Figure 6.7 and 6.8c–d includes these warm streamer effects, and that warm streamers in the Kuroshio Extension region are one of the final supply routes to the surface for nutrients transported by the Kuroshio.

6.5. DIAPYCNAL MIXING PROCESSES ALONG THE KUROSHIO

As opposed to the eddy-induced along-isopycnal stirring effects, diapycnal upward nutrient transport acts to enhance and maintain the along isopycnal nutrient anomaly along the Kuroshio nutrient stream. One of the most likely mixing "hotspots" along the Kuroshio is in the Kuroshio upstream, in the Okinawa Trough and the Tokara Strait. In these regions, the Kuroshio has to flow over shallow topography and narrow straits between islands and steep seamounts. Downstream, there is also a large seamount with a number of islands in Izu-Ogasawara Ridge south of Tokyo (Hasegawa, Chapter 10 this book). No such topographic obstacles are present in the Gulf Stream except the Bahama Banks (Gula et al., 2016) and the New England Seamounts (Cornillon, 1986; Ezer, 1993).

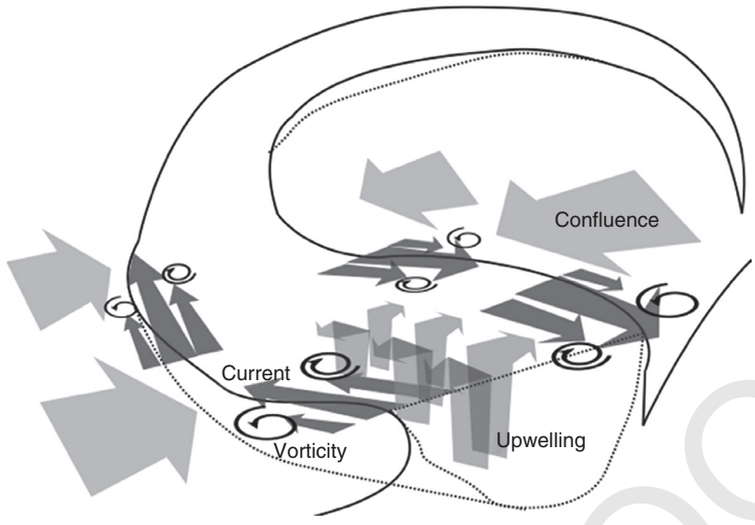

Figure 6.10 Schematics of the warm streamer under the frontogenetic confluence.

6.5.1. Observations of Diapycnal Mixing in the Tokara Strait

In a previous study of the Kuroshio, large amplitude near-inertial internal waves of high vertical wavenumber were observed in the Okinawa Trough and the Tokara Strait near the Kuroshio, and in the region between the Kuroshio and the continental shelf. These internal waves likely induce strong turbulent mixing (Rainville & Pinkel, 2004). Recent microstructure experiments showed strong turbulent mixing associated with near-inertial internal waves of very small vertical wavelength, O(50 m) near islands and seamounts (Tsutsumi et al., 2017). However, direct turbulence measurements are still scarce in this region. Nagai et al. (2017) conducted a quasi freefall tow-yo microstructure experiment, using an Underway-VMP (UVMP) in the Tokara Strait during November 2016 aboard the R/T/V Kagoshima-maru. The measured zonal velocity shear using a shipboard Acoustic Doppler Current Profiler (ADCP, 75 kHz 30° beam angle, Ocean Surveyor, Teledyne RDI), which is back-rotated at the local inertial frequency to a reference time, shows banded structures of high vertical wavenumber alternating positive and negative values following closely along the isopycnal. This suggests the propagation of near-inertial internal waves (Figure 6.11a). Hodographs and rotary spectra indicate that the energy of these waves propagate in the upward and downward directions (Nagai et al., 2017).

In this large amplitude high vertical wavenumber near-inertial internal wave field, we have succeeded in making direct turbulence measurements at very high lateral resolution, ~1–2 km, down to 300 m depth. The measured turbulent kinetic energy dissipation rates show bands of coherent strong turbulent layers (Figure 6.11b) clearly associated with the observed banded near-inertial internal wave shear (e.g., 129.35-129.55°E along $\sigma_\theta = 23$ kgm^{-3}; 129.35-129.45°E along $\sigma_\theta = 25$ kgm^{-3}; 129.47-129.65°E along $\sigma_\theta = 24.5$-25 kgm^{-3}; 129.56-129.65°E along $\sigma_\theta = 26$ kgm^{-3}; Figure 6.11a, 6.11b). The banded turbulent layers spread horizontally with a lateral scale of over O(10 km). These results suggest that the frequently observed dominant near-inertial internal wave shear in previous studies is actively breaking into three-dimensional turbulence. This creates widespread subsurface active mixing layers in the Kuroshio upstream. The upper 500 m averaged relative vorticity shows that the large amplitude internal wave shear and associated strong turbulence are in the region of negative relative vorticity of the Kuroshio (Figure 6.12), similar to previous studies (Kunze, 1985). This suggests that the Kuroshio acts as a catalyst to dissipate near-inertial internal waves propagating near the Tokara Strait. The estimated eddy diffusivities using measured turbulent kinetic energy dissipation rates with background buoyancy frequency show average values of O(10^{-4} m^{2}s^{-1}) below 100 m depth. Although our turbulence measurements only reach the upper edge of the North Pacific Intermediate Water (NPIW) density layer, the average subsurface diffusivity of O(10^{-4} m^{2}s^{-1}) is consistent with the previously estimated values (Nakamura et al., 2014) for diapycnal diffusivity for water mass modification of the NPIW in this region using long-term salinity records. In addition to water mass mixing, the observed turbulent mixing is important for driving upward nutrient fluxes, since the Kuroshio carries a large amount of nutrients in its subsurface layer ($\sigma_\theta = 24$–27 kg m^{-3}) in this region (Chen, 1996; Guo et al., 2012).

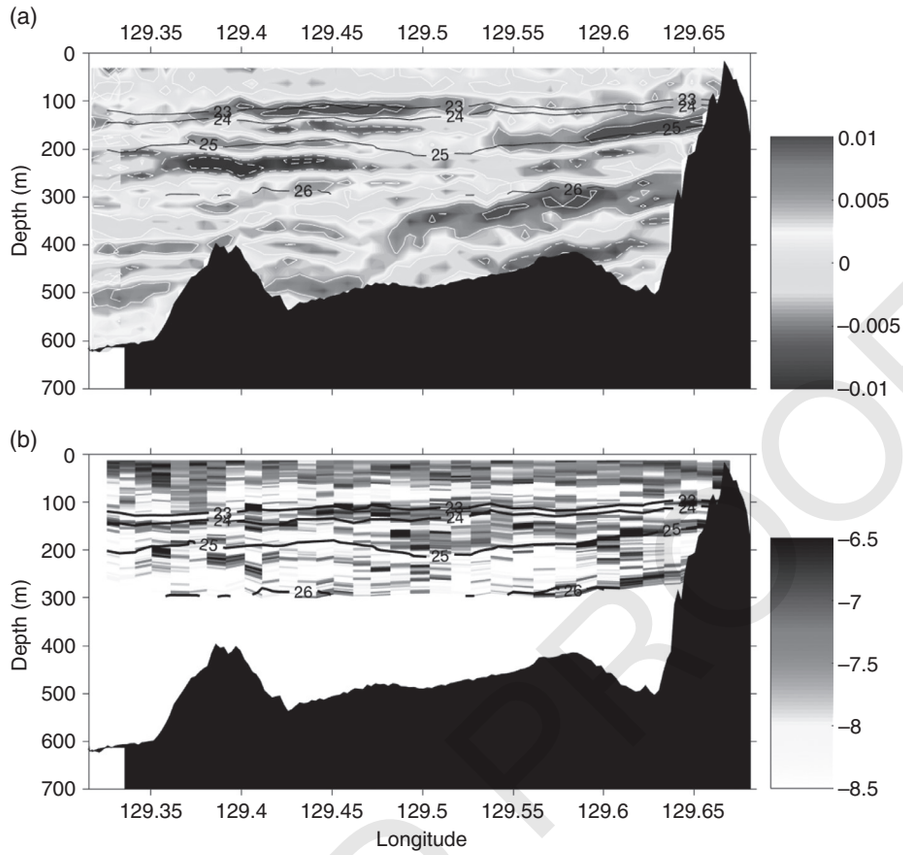

Figure 6.11 ADCP vertical shear of the zonal current, back-rotated with the local Coriolis frequency (s^{-1}) is shown in (a) (white solid contour) positive and (white dashed contour) negative values. (b) Measured turbulent kinetic energy dissipation rates in log scale ($W kg^{-1}$) in the Tokara Strait during November 2016 R/T/V Kagoshima-maru cruise. Black contour represents isopycnal.

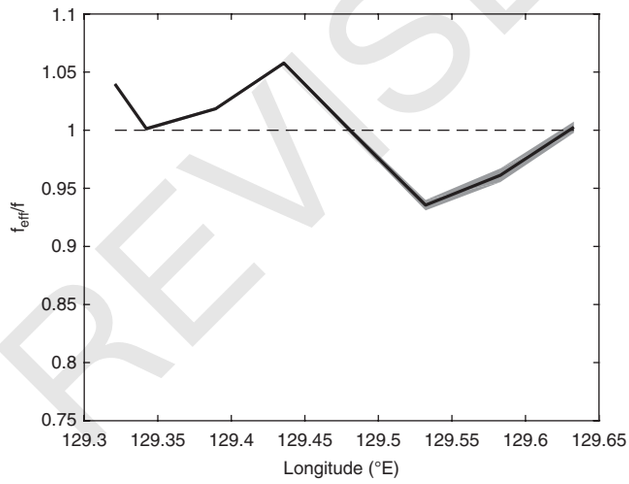

Figure 6.12 Normalized effective Coriolis frequency (Kunze, 1985) by local Coriolis frequency averaged within the upper 500 m as a function of longitude. Shading represents 95 % confidence interval for each average value. Horizontal dashed line indicates unity.

Wind energy is the main source of these near-inertial internal waves. The estimated wind power input to produce near-inertial oscillations using a slab model suggests that wind input is sufficient to produce the observed near-inertial internal wave vertical energy flux of O(0.1-1 m Wm^{-2}) (Nagai et al., 2017). However, it is unclear how the observed high vertical wavenumber near-inertial internal waves are generated. The study region is close to the so-called critical latitude, 28.9°N, where the semidiurnal M_2 internal tide energy can be efficiently converted to that of the near-inertial internal waves of high vertical wavenumber through parametric subharmonic instability (PSI) (MacKinnon & Winters, 2005). Relatively long-term ADCP observations in the same region during 2001-2002 suggest that near-inertial shear amplitude modulates fortnightly similar to that of tidal forcing. This suggests that PSI may be a source for the observed high vertical wavenumber near-inertial internal waves (Qiu et al., 2012; Nagai et al., 2017). However, the near-inertial shear amplitude is correlated better with the external diurnal tidal forcing ($D_1 = K_1 + O_1$)

than that of semidiurnal components ($D_2 = M_2 + S_2 + N_2$). The location of the study site is at ~30°N, north of the critical latitude, where the diurnal internal tides are also near-inertial internal waves. Thus, observed high vertical wavenumber near-inertial internal waves might also be generated by diurnal tides over nearby seamounts. Previous studies have also shown that the geostrophic flow over topography can generate near-initial internal waves (Nikurashin & Ferrari, 2011). Globally estimated, this lee wave generation rate in the Kuroshio upstream is O(0.1–1 m Wm^{-2}) (Nikurashin & Ferrari, 2011), consistent with our estimates above. Because the Kuroshio flows over shallow topography in the Okinawa Trough and the Tokara Strait, this mechanism cannot be ruled out.

6.5.2. Banded Shear and Strong Turbulence in the Thermocline of the Downstream Kuroshio Extension

Even without wind, tides, and topography, meandering strong fronts can generate spontaneously high vertical wavenumber near-inertial internal waves (Snyder et al., 1993; Plougonven & Snyder, 2005, 2007; Alford et al., 2013; Nagai et al., 2015a; Shakespeare & Taylor, 2014; Shakespeare & Hogg, 2017). Results from numerical simulations of the meandering Kuroshio Extension without surface forcing reproduce high vertical wavenumber near-inertial internal waves in the thermocline of the Kuroshio, consistent with observations (Nagai et al., 2015a). However, semi-Lagrangian analyses for an internal wave energy equation suggest that most of the generated internal wave energy is reabsorbed into the mean flow due to a strong mesoscale confluence (Nagai et al., 2015a). Using the observation data, Nagai et al. (2009; 2012; 2015a) showed that the banded shear is frequently observed in the thermocline of the Kuroshio Extension; it is attributed to the propagating internal waves (Figure 6.13a). Simultaneously measured microscale turbulent kinetic energy dissipation rates show very large values of O(10^{-7}–10^{-6} W kg^{-1}), 100-1000 times greater than typical open water thermocline values (Figure 6.13c). These observed banded shears could be caused by trapped and amplified wind-induced internal waves (Kunze, 1985; Whitt & Thomas, 2013; Whitt et al., 2018), and are not necessarily due to spontaneously generated near-inertial internal waves. However, regardless of their generation mechanisms, the microstructure observations suggest that these banded internal wave shears enhance diapycnal turbulent mixing in the thermocline of the Kuroshio. Internal wave induced mixing in the Kuroshio thermocline can be an important process for the upward diffusion of nutrients transported through the Kuroshio nutrient stream.

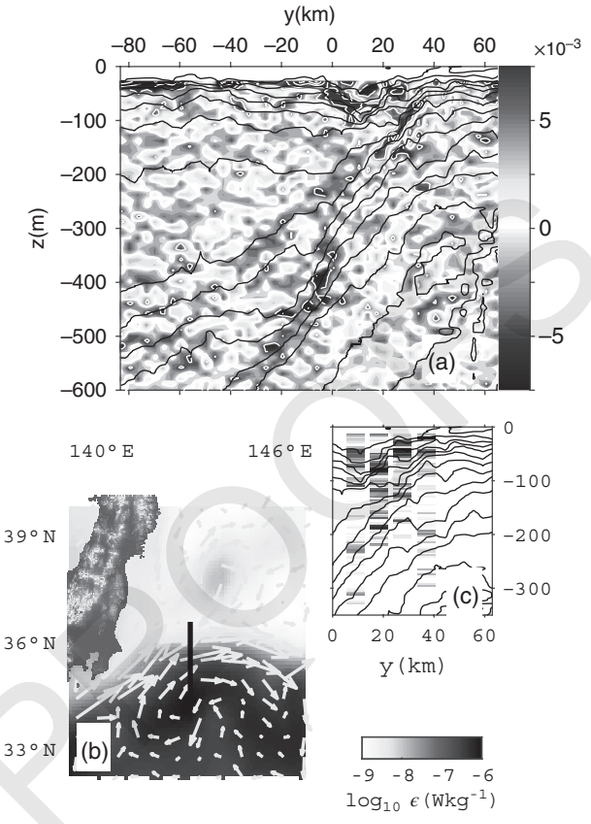

Figure 6.13 (a) The residual shear with (white solid contour) positive and (white dashed contour) negative values, computed by subtracting the geostrophic shear from the total shear measured during August 2011 along the meridional direction as in (b). Measured TKE dissipation rates ε in log scale (W kg^{-1}) are shown in (c). Note that panel (a) and (c) are aligned with the same lateral position to compare the locations of the strong shear and dissipation rates.

6.5.3. Double-Diffusive Convection in and below the Thermocline of the Kuroshio Extension

Even without turbulence, seawater can be mixed diapycnally by double-diffusive convection. Oschlies et al. (2003) estimated the salt-finger induced nitrate diapycnal vertical flux using a salt-finger diffusivity parameterization in an eddy permitting model of the Atlantic. The results suggest that the basin-wide average nitrate flux due to salt-fingers accounts for 0.08 mmol N m^{-2} day^{-1}, which is equivalent to the average turbulent and mesoscale eddy-induced vertical nitrate fluxes estimated by Oschlies (2002). The parameterized salt-finger induced diffusivities in the model are O(10^{-5} m^2s^{-1}) on average (Table 1 of Oschiles et al., 2003). These results suggest that salt-fingers could be an important diapycnal mixing process for vertical nutrient flux. However, because the resolution of the numerical model was eddy permitting at

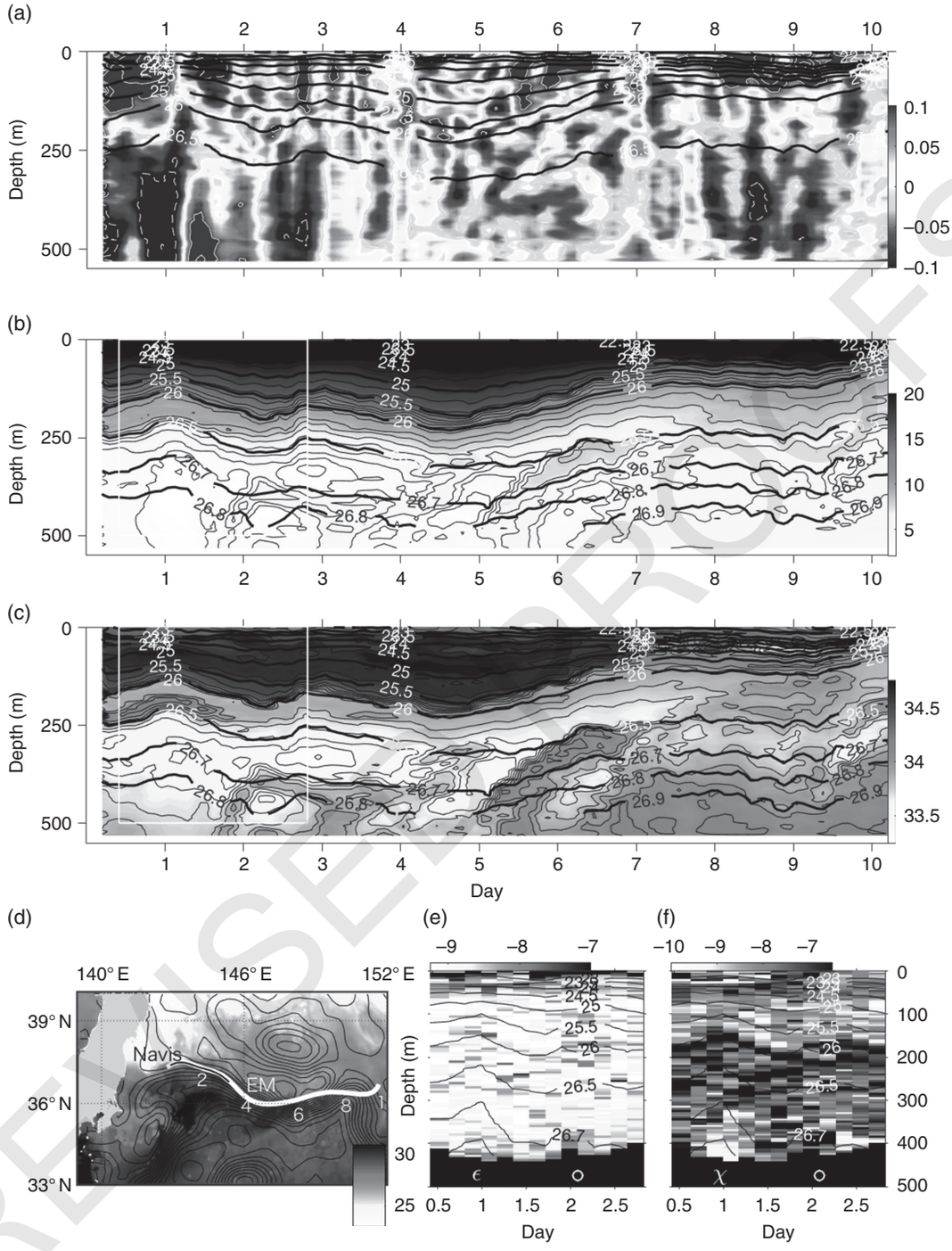

Figure 6.14 (a) Across front velocity measured by the EM-APEX Float deployed along the Kuroshio Extension with (white solid contour) positive and (white dashed contour) negative values. The trajectory of the float is seen in (d). Measured temperature and salinity are shown in (b) and (c). Microscale turbulent kinetic energy dissipation rates ε ($W\,kg^{-1}$) and thermal variance dissipation rates χ($K^2\,s^{-1}$) are shown in log scale in (e) and (f), respectively.

~0.3°, the fine-scale thermohaline interleaving structures in the simulation might be largely underestimated. The Lagrangian rate of change of the density ratio R_ρ can be expressed as:

$$\frac{DR_\rho}{Dt} = \frac{(R_\rho - 1)}{S_z}\left(\frac{\partial u_i}{\partial z}\frac{\partial S}{\partial x_i} + \frac{\partial v_i}{\partial z}\frac{\partial S}{\partial y_i}\right) - \text{Mixing Terms} \tag{6.2}$$

where x_i and y_i are the zonal and meridional coordinates on the density surface, respectively, z the vertical coordinate, S salinity, S_z the salinity vertical gradient, and R_ρ is the density ratio defined as $R_\rho = \alpha\Theta_z / \beta S_z$, where α is the thermal expansion coefficient, β the salinity contraction coefficient, θ_z the vertical temperature gradient, and the Mixing Terms represent all of the diffusion terms (Schmitt, 1990). Equation (6.2) illustrates that the products of the vertical shear and salinity along isopycnal gradients are the critical terms to tilt the existing thermohaline anomaly to change R_ρ. Accordingly, the model still needs to resolve fine-scale vertical shear associated with mesoscale and submesoscale flows and internal waves to evaluate the contributions from double-diffusive convection to tracer mixing.

Along the Kuroshio nutrient stream, the along-isopycnal thermohaline anomaly is enhanced after it reaches the Kuroshio Extension, where cold low-salinity water of the subpolar region is advected to the south by the Oyashio current to encounter the warm salty Kuroshio waters. In July 2013, an Electro-Magnetic Autonomous Profiling Explorer Float (EM-APEX float) was deployed along the Kuroshio Extension axis from the R/V *Kaiyo* (Nagai et al., 2015b) to measure current velocity, temperature, salinity, and pressure down to 500 m depth every two hours. An autonomous microstructure profiling float (Navis-MicroRider: Navis-MR) equipped with two shear probes, two FP07 thermistors, and CTD sensors was also deployed, along the same trajectory as the EM-APEX float, to record upper 500 m microstructure data every three hours (Nagai et al., 2015b). The EM-APEX float and the Navis-MR float measured these data over 900 km in 10 days and over 300 km in 3-4 days, respectively, along the Kuroshio Extension.

The temperature and salinity data obtained by the EM-APEX float showed fine-scale vertical inversions below 150 m depth over the entire 900-km trajectory (Figure 6.14b, 6.14c). These thermohaline interleaving structures are found to be favorable for active salt-finger and diffusive-convection of double-diffusion, based on the computed Turner angle (Figure 5 in Nagai et al., 2015b).

The measured microscale turbulent kinetic energy dissipation rates were small, O(10^{-10}–10^{-9} W kg^{-1}) with a few moderate values of O(10^{-8} W kg^{-1}) (Figure 6.14e). On the other hand, microscale dissipation rates of temperature variance measured by the Navis-MR, showed very large values of O(10^{-7}-10^{-6} K^{2}s^{-1}) below 150 m depth over 300 km, where fine-scale thermohaline interleaving structures were formed (Figure 6.14f). The combination of weak turbulence, strong thermal dissipation rates, and double-diffusion favorable thermohaline conditions are indicative of the active occurrence of double-diffusive convection. The average effective thermal diffusivity below 150 m depth is computed by

$$K_\theta = \frac{\chi}{2\overline{\Theta_z}^2} \tag{6.3}$$

where χ is the microscale thermal variance dissipation rate, and $\overline{\Theta_z}$ is the mean temperature vertical gradient (Osborn & Cox, 1972). The effective thermal diffusivity shows O(10^{-3} m^{2}s^{-1}), which is 100 times greater than the eddy diffusivity for density (Nagai et al., 2015b) based on the measured turbulent kinetic energy dissipation rates, illustrating that double-diffusion is more important than turbulence below 150 m depth along the Kuroshio Extension. Additionally, the thermal diffusivities based on the microstructure measurements are two orders of magnitudes larger than those estimated by the eddy permitting model of Oschiles et al. (2003). These subsurface layers correspond to the density layers of σ_θ = 25–27 kg m^{-3}, where the core of the Kuroshio nutrient stream flows. Our measurements clearly show that the active double-diffusive convection, observed below the Kuroshio Extension, plays a very important role in mixing the nutrients upwards into the euphotic layer. Coherence analysis between the observed density ratio R_ρ and the shear measured using the EM-APEX float showed a high correlation at subinertial and inertial frequencies (Nagai et al., 2015b). High correlations at the subinertial frequency correspond to a combination of mesoscale shear and thermohaline variations caused by the meandering of the Kuroshio Extension. High correlations at the inertial frequency correspond to the dominant near-inertial wave shear (Figure 6.14a) and associated fine scale thermohaline interleaving (Figure 6.14, 6.14c). These results suggest that the vertical shear in equation (6.2) caused by both subinertial flows due to meso and submesoscale meandering of the Kuroshio Extension, and that of near-inertial internal waves, act to catalyze active microscale double-diffusive convection.

6.6. NUTRIENT SUPPLY PROCESS OF THE KUROSHIO NUTRIENT STREAM ON THE SOUTH SIDE OF THE KUROSHIO EXTENSION

As noted in the Introduction (section 6.1), the large amount of nutrients transported by the Gulf nutrient stream is supplied to the surface mixed layer through induction. The induction process is also thought to

supply nutrients to the surface euphotic layer of the Kuroshio nutrient stream (Komatsu, Chapter 5 this book). However, as mentioned in sections 6.1 and 6.2, the final supply regions of the Kuroshio nutrient stream are the Kuroshio Extension region and the Kuroshio–Oyashio confluence, where meso and submesoscale eddies and filaments likely stir nutrients in the lateral direction. The microscale turbulence and inorganic nutrient measurements were made across the Kuroshio Extension aboard the R/V *Natsushima* (Nagai et al., 2012). These observations were made in the fall, when the mixed layer was developed as deep as 60–70 m on the southern side of the Kuroshio Extension, whereas on the northern side, the mixed layer was much shallower at ~10 m. One of the most striking features observed was a tongue-like structure in the nutrient concentrations, extending for approximately 30 km at ~60 m depth from north to south, below the mixed layer on the southern side of the Kuroshio Extension (Clayton et al., 2014; Figure 6.15b). This interleaving structure originated from the along-isopycnal maximum concentration of nitrate formed to the north of the Kuroshio Extension nutrient stream (see also Figure 6.4).

The microstructure data also showed strong turbulence within the surface mixed layer on the southern side of the Kuroshio Extension. This was attributed to downfront wind stress that occurred during the cruise (Nagai et al., 2012). Previous studies have shown that downfront winds can change the sign of Ertel's potential vorticity and induce symmetric instability (Thomas & Lee, 2005) and three-dimensional turbulence in the Kuroshio Extension front (D'Asaro et al., 2011). The downfront wind induced mixing is known to generate a lens of homogeneous low PV water, which is subducted along isopycnals. This subduction process could play a role in forming the observed nitrate tongue; however, because the nitrate interleaving is found in the high PV stratified layer below the mixed layer, downfront wind induced subduction is an unlikely candidate as a generation mechanism for the nitrate interleaving. The observed vigorous turbulence caused by the downfront wind in the mixed layer on the south side of the Kuroshio Extension, above the nitrate interleaving structures, can entrain nitrate into the mixed layer. The estimated turbulent vertical diffusive nitrate flux is O(1 mmol N m^{-2} day^{-1}), consistent with the satellite chlorophyll-based estimates of primary production in this region during October 2009 (Nagai & Clayton, 2017).

To investigate the mechanisms responsible for forming nitrate interleaving structures, a numerical simulation was conducted using the North Pacific configurations of ROMS coupled with the N_2PZD_2 ecosystem model (Nagai & Clayton, 2017), similar to that described in Section 6.2. A nested grid with lateral resolution of 2 km was embedded in the Kuroshio Extension region and the model was forced with JRA-55 6-hourly reanalysis winds, including those from the observation period. The simulation for October 2009 reproduced prominent warm streamers extending from the first meander crest to the warm core ring on the north of the Kuroshio Extension. This compared favorably with the October 2009 observations (Nagai et al., 2012; Nagai & Clayton, 2017). On the southern side of the front, the simulations showed nitrate interleaving structures extending from the north below the mixed layer, with length scales similar to those of the observations. The Lagrangian rate of change in the vertical nitrate gradient, which may be a measure of nitrate interleaving tendency, can be expressed similar to equation (6.2):

$$\frac{D}{Dt}\left(\frac{\partial NO_3^-}{\partial z}\right)=-\left(\frac{\partial u}{\partial z}\frac{\partial NO_3^-}{\partial x}+\frac{\partial v}{\partial z}\frac{\partial NO_3^-}{\partial y}+\frac{\partial w}{\partial z}\frac{\partial NO_3^-}{\partial z}\right)-M+B \tag{6.4}$$

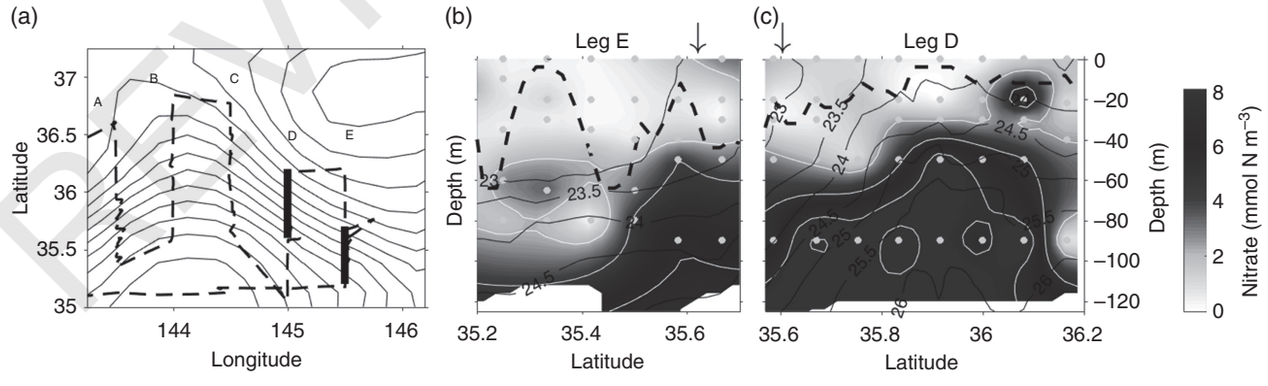

Figure 6.15 (a) Ship track observations made by the R/V Natsushima during October 2009 is shown as dashed line. The thick black lines in (a) indicate the meridional ranges shown in (b) and (c). Black contours are sea surface height every 0.1 m in (a). (b) and (c) are the vertical section of the nitrate concentration (m mole N m^{-3}) in Leg E and D, respectively. The surface mixed layer depth is shown by the thick dashed black line. Black contours in (b–c) are σ_θ.

where NO_3^- is the nitrate concentration, *x, y, z* are zonal, meridional, and vertical coordinates, and *u, v, w* are zonal, meridional, and vertical velocities, respectively, *M* is the mixing term, and *B* is the biological sink/source. The first two terms on the right- hand side, the product of vertical shears and lateral nitrate gradients, can be split into three parts: geostrophic, ageostrophic, and internal wave fluctuations. The residual shear, $\partial \mathbf{u}_r/\partial z$, which includes ageostrophic subinertial shear and internal wave shear, can be obtained by subtracting the 30-hour averaged geostrophic shear $\partial \mathbf{u}_g/\partial z$ from the total shear $\partial \mathbf{u}/\partial z$ in the Eulerian frame, to give:

$$\frac{\partial \mathbf{u_r}}{\partial z} = \frac{\partial \mathbf{u}}{\partial z} - \frac{\partial \mathbf{u_g}}{\partial z} \tag{6.5}$$

These residual shear and lateral nitrate gradients can be further split into subinertial ageostrophic and internal wave fluctuation components along the Lagrangian trajectories of the water parcels. Specifically, the 30-hour average of residual shear and that of the lateral nitrate gradient along the Lagrangian particle trajectories are subtracted from the instantaneous residual shear and the lateral nitrate gradients, respectively, to obtain internal wave shear and the lateral nitrate gradient fluctuations due to internal waves. The resultant Lagrangian rate of change in the nitrate vertical gradient becomes:

$$\overline{\frac{D}{Dt}\frac{\partial NO_3}{\partial z}} = -\overline{\frac{\partial \mathbf{u_g}}{\partial z}} \cdot \overline{\nabla_h NO_3} - \overline{\frac{\partial \mathbf{u}_a}{\partial z}} \cdot \overline{\nabla_h NO_3} - \overline{\frac{\partial \mathbf{u}_{IW}}{\partial z} \cdot \nabla_h NO_3} - \overline{\frac{\partial w}{\partial z}\frac{\partial NO_3}{\partial z}} - M + B. \tag{6.6}$$

where the overbar represents the 30-hour average, $\mathbf{u}_a$ ageostrophic velocity, $\mathbf{u}_{IW}$ internal wave velocity. Note that the sum of the resultant three components of shear, lateral nitrate gradients, and their covariance recover each original instantaneous term. To evaluate each term of equation (6.6) along the simulated Lagrangian trajectories, 25,000 passive Lagrangian particles were released in the model three-dimensional flow field. The results show that subinertial ageostrophic shear is the dominant term in modifying the vertical nitrate gradient compared to other shear terms. While the near-inertial internal wave shear generated by a six-hourly wind can induce large amplitude fluctuations of the vertical nitrate gradient, they only strengthen and weaken the gradient back and forth at near-inertial frequencies and do not influence the formation of the nitrate interleaving structures (Nagai & Clayton, 2017). However, as discussed in section 6.5.3, the near-inertial shear is effective in acting as a catalyst to produce active double-diffusive convection. The model used in this study does not include the double-diffusive convection parameterization and so may underestimate the contributions from the near-inertial internal wave shear.

6.7. SUMMARY AND CONCLUSION

Results from recent observations and numerical simulations of the Kuroshio nutrient stream and related diapycnal mixing processes, important for the lateral and vertical nutrient supply in the Kuroshio region, are summarized here.

We have employed a basin-scale eddy permitting numerical model of the Kuroshio region to reproduce the Kuroshio nutrient stream. We found our model results to be consistent with World Ocean Atlas and regional observations of nitrate distributions in the Kuroshio. The major source of nitrate transported by the Kuroshio nutrient stream is found to be at the tropical regions of western North Pacific on the south side of the North Equatorial Current at ~15°N.

We found that the Kuroshio nutrient stream transports a large amount of nitrate to Japanese coastal waters, forming a mostly positive meridional gradient of nitrate along density surfaces off Honshu Island. After the Kuroshio flows away from the coast to the Kuroshio Extension region, the meridional along-isopycnal nitrate gradient becomes negative on the north of the Kuroshio nutrient stream. These regional differences in the along-isopycnal nitrate gradient result in different patterns of eddy-induced nitrate fluxes. Off Honshu Island, the positive along-isopycnal meridional nitrate gradient means that eddy-induced fluxes tend to remove the nitrate-rich waters from between the Kuroshio and the coast, transporting them to the south and into deep subsurface layers. On the other hand, in the Kuroshio Extension region where the along-isopycnal meridional nitrate gradient has both signs, positive on the south side, and negative on the north, the eddy-induced nitrate flux is directed upward and northward on the north side, and downward and southward on the south side of the Kuroshio Extension. These results are consistent with theoretical and numerical studies which show that eddies are responsible for homogenizing existing along isopycnal tracer anomalies (Rhines & Young, 1982; Lee & Williams, 2000; Gruber et al., 2011; Nagai et al., 2015c).

Recent in situ microstructure observations, for example Tsutsumi et al. (2017) and Nagai et al. (2017), show that the upstream Kuroshio regions, the Okinawa Trough and the Tokara Strait, are "mixing hotspots". The observed banded coherent layers of strong turbulence are attributed to the breaking of propagating high vertical wavenumber near-inertial internal waves. The Kuroshio appears to be a catalyst for energy dissipation and diapycnal mixing by trapping the near-inertial internal waves in the regions of anticyclonic vorticity (Nagai et al., 2017).

The banded near-inertial shear and associated enhanced turbulent mixing are frequently observed not only in the upstream Kuroshio, but are also seen with moderate amplitudes in the downstream Kuroshio Extension thermocline. These banded shears and elevated turbulence in the Kuroshio thermocline could be intrinsic characteristics, which might promote the upward flux of nutrients to form and/or maintain streaks of relatively higher nutrient concentrations along the Kuroshio nutrient stream. In addition, under the Kuroshio Extension thermocline there are widespread thermohaline interleaving structures that are likely generated by vertical shear of subinertial flows and near-inertial internal waves. The observed large microscale thermal variance dissipation rates of $O(10^{-7}\text{-}10^{-6}\ K^2 s^{-1})$ and thermal diffusivity $O(10^{-3}\ m^2 s^{-1})$ with weak turbulence and double-diffusion favorable thermohaline interleaving structures suggest active double-diffusive convection. Since these subsurface layers ($\sigma_\theta = 25\text{-}27\ kg\,m^{-3}$) include the core of the nutrient stream, double-diffusion could act as an important agent for diffusing nutrients up into the euphotic zone.

During the fall, when the mixed layer deepens to form a mixed layer front on top of the Kuroshio Extension, subinertial ageostrophic and geostrophic vertical shears are found to be effective in forming nitrate interleaving structures. Observations suggest that these nitrate "tongues" can extend from the Kuroshio Extension nutrient stream to the south below the mixed layer with lateral scales of O(10 km) and vertical scales of O(10 m). The interleaving nitrate layers can then be entrained into the surface mixed layer on the southern side of the front by strong upper layer turbulence driven by downfront wind stress. The diapycnal turbulent nitrate flux is estimated to be $O(1\ mmol\ N\ m^{-2}\ day^{-1})$.

The results of this study indicate that the Kuroshio is likely to play multiple roles in supplying nutrients laterally and vertically through multiscale processes (Figure 6.16, Table 6.1). At the largest scale, the Kuroshio acts as a basin-scale subsurface nutrient conduit that transports large amounts of nutrients from the tropical ocean to the Kuroshio Extension and the Kuroshio–Oyashio confluence. There should be little loss by biological uptake of nutrients transported in the dark subsurface of the Kuroshiro, and there should be some gain through the smallest process of diapycnal turbulent mixing, especially when the Kuroshio passes over shallow topographic features, such as the Okinawa Trough and

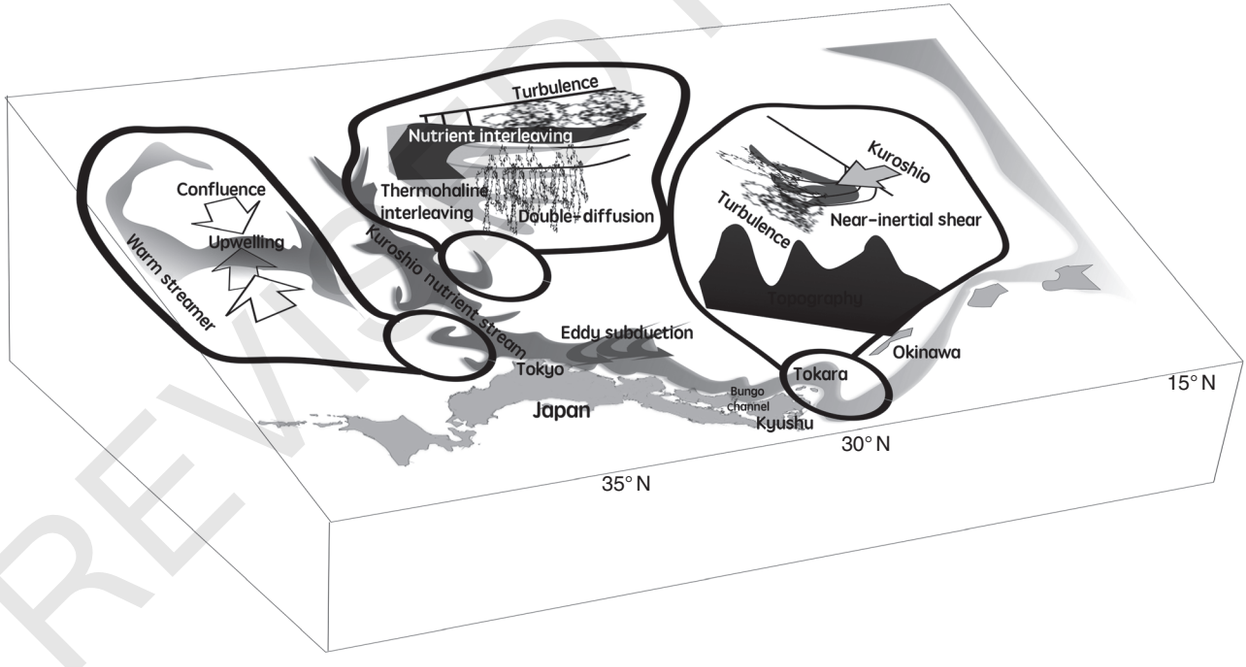

Figure 6.16 Schematic of the multiscale routes for nutrient supply. The basin-scale Kuroshio nutrient stream flows over shallow topography in the Okinawa Trough and the Tokara Strait, where strong turbulent mixing can mix nutrient upward. The warm core eddies and warm filaments on the northern side of the Kuroshio Extension may transport nutrient within the Kuroshio nutrient stream upward and northward. On the southern side, meso and submesoscale shears produce nutrient interleaving structures, which can be entrained into the surface mixed layer. In and below the thermocline of the Kuroshio Extension, thermohaline interleaving structures formed by meso, submesoscale and near-inertial wave shears, enhance the double-diffusion, which could diffuse nutrient upward. (*See insert for color representation of this figure*.)

Table 6.1 Summary Table for the Expected Nutrient Flux Along and Across the Kuroshio Path*.

Locations along and across the Kuroshio	Dense (coastal/north) side	Kuroshio axis	Light (offshore/south) side
Upstream Okinawa Tokara		Very strong ↑ upward diapycnal flux by microscale turbulence	
South of Honshu	↑ Upward and ← onshore flux by Kuroshio induced bottom cold water intrusion events to the coastal seas	Moderately strong ↑upward diapycnal flux by microscale turbulence	↓ Downward and → offshore flux by mesoscale eddies and filaments
Kuroshio Extension	↑ Large upward and ← northward flux by mesoscale eddies and filaments	Strong ↑ upward flux by double-diffusive convection. Moderately strong ↑ upward diapycnal flux by microscale turbulence	↓ Downward and → southward flux by mesoscale eddies and filaments (may induce nutrient tongues below the mixed layer front)

*Suggested by the results from the present study. Blank indicates that it is yet to be known. The arrow ↑ represents upward flux, ↓ downward flux, ← onshore/northward flux, → offshore/southward flux.

the Tokara Strait. Another microscale process, double-diffusive convection in and below the thermocline of the Kuroshio Extension is found to be an important diapycnal mixing process. These double-diffusion favorable thermohaline interleaving structures in the Kuroshio Extension are actively produced by the next two largest-scale flows, mesoscale, submesoscale and near-inertial internal wave shears. These mesoscale and submesoscale shears also stir the positive nutrient anomalies on the density surfaces associated with the Kuroshio nutrient stream to form nutrient interleaving structures on the southern side of the Kuroshio Extension front, which are then entrained into the surface mixed layer by enhanced turbulence by downfront winds (Figure 6.16, Table 6.1).

Although the observations and the numerical simulations described in this study provide evidence for these multiscale nutrient supply process, many of these nutrient fluxes are not well quantified, especially for the diapycnal nutrient fluxes. This is primarily due to a lack of sufficient simultaneous observations of nutrients and microstructures. Although the Kuroshio nutrient stream is a basin-scale phenomenon, the interannual variations in the nutrient stream have yet to be investigated sufficiently. More intensive in situ observations of simultaneous microstructures and nutrients, and basin-scale high resolution numerical simulations using proper mixing parameterizations for internal waves and double-diffusion are necessary in the near future to address these issues.

REFERENCES

Alford, M. H., A. Y. Shcherbina, & M. C. Gregg (2013), Observations of near-inertial gravity waves radiating from a frontal jet, *Journal of Physical Oceanography*, *43*, 1225–1239.

Arai, M. (2005), Numerical study of a Kyucho and a bottom intrusion in the Bungo Channel, Japan: Disturbances generated by the Kuroshio small meanders, *Journal of Oceanography*, *61*, 953–971.

Chen, C. T. A., (1996) The Kuroshio intermediate water is the major source of the nutrients on the East China Sea continental shelf, *Oceanologica Acta*, *19*, 523–527.

Chen, C. T. A., C. T. Liu, &S. C. Pai (1995), Variations in oxygen, nutrient and carbonate fluxes of the Kuroshio Current, *La Mer*, *33*, 161–175.

Clayton, S., T. Nagai, & M. J. Follows (2014), Fine scale phytoplankton community structure across the Kuroshio Extension Front, *Journal of Plankton Research*, *36*, 1017–1030, https://doi.org/10.1093/plankt/fbu020.

Cornillon, P. (1986), The effect of the New England Seamounts on Gulf Stream meandering as observed from satellite IR imagery, *Journal of Physical Oceanography 16*, 386–389.

D'Asaro., E., C. Lee, L. Rainville, L. Harcourt, & L. Thomas (2011), Enhanced turbulence and energy dissipation at ocean fronts, *Science*, *332*, 318–322. https://doi.org/10.1126/science.1201515

da Silva, A., A. C. Young, & S. Levitus (1994), Atlas of surface marine data 1994, Algorithms and procedures. Technical Report 6, Department of Commerce, NOAA, NESDIS.

Ezer, T. (1994), On the interaction between the Gulf Stream and the New England Seamount Chain, *Journal of Physical Oceanography 24*, 191–204.

Garcia, H. E., R. A. Locarnini, T. P. Boyer, J. I. Antonov, O. Baranova, M. Zweng, et al. (2014), *World Ocean Atlas 2013*, Volume 4: Dissolved Inorganic Nutrients (phosphate, nitrate, silicate).

Gruber, N., H. Frenzel, S. C. Doney, P. Marchesiello, J. C. McWilliams, J. R. Moisan, et al. (2006), Eddy-resolving simulation of plankton ecosystem dynamics in the California Current System, *Deep-Sea Research I*, *53*, 1483–1516.

Gruber, N., Z. Lachkar, H. Frenzel, P. Marchesiello, M. Münnich, J. C. McWilliams, et al. (2011), Eddy-induced reduction of biological production in eastern boundary upwelling systems, *Nature Geoscience*, *4*, 787–792.

Gula, J., M. J. Molemaker, & J. C. McWilliams (2016), Topographic generation of submesoscale centrifugal instability and energy dissipation, *Nature Communications*, *7*, 12811, https://doi.org/10.1038/ncomms12811.

Guo, X., X. H. Zhu, Y. Long, & D. Huang (2013), Spatial variations in the Kuroshio nutrient transport from the East China Sea to south of Japan, *Biogeosciences*, *10*, 6403–6417.

Guo, X., X. H. Zhu, Q. S. Wu, & D. Huang (2012), The Kuroshio nutrient stream and its temporal variation in the East China Sea, *Global Biogeochemical Cycles*, *117*, C01,026, https://doi.org/10.1029/2011JC007292.

Inoue, R., M. C. Gregg, & R. R. Harcourt (2010), Mixing rates across the Gulf Stream, Part 1: On the formation of Eighteen Degree Water, *Journal of Marine Research*, *68*, 643–671.

Kaneda, A., H. Takeoka, E. Nagaura, & Y. Koizumi (2002), Periodic intrusion of cold water from the Pacific ocean into the bottom layer of the Bungo Channel in Japan, *Journal of Oceanography*, *58*, 547–556.

Kaneko, H., I. Yasuda, K. Komatsu, & S. Itoh (2012), Observations of the structure of turbulent mixing across the Kuroshio, *Geophysical Research Letters*, *39*, https://doi.org/10.1029/2012GL052419.

Kaneko, H., I. Yasuda, K. Komatsu, & S. Itoh (2013), Observations of vertical turbulent nitrate flux across the Kuroshio, *Geophysical Research Letters*, *40*, 3123–3127, https://doi.org/10.1002/grl.50613.

Klein, P., & G. Lapeyre (2006), The oceanic vertical pump induced by mesoscale and submesoscale turbulence, *Annual Review of Marine Science*, *1*, 351–375.

Kunze, E. (1985), Near-inertial wave propagation in geostrophic shear, *Journal of Physical Oceanography*, *15*, 544–565.

Lee, M.-M., & R. G. Williams (2000), The role of eddies in the isopycnic transfer of nutrients and their impact on biological production, *Journal of Marine Research*, *58*, 895–917.

Levy, M., P. Klein, & G. Madec (2001), Impacts of sub-mesoscale physics on phytoplankton production and subduction, *Journal of Marine Research*, *59*, 535–565.

MacKinnon, J. A., & K. B. Winters (2005), Subtropical catastrophe: Significant loss of low-mode tidal energy at 28.9°, *Geophysical Research Letters*, *32*, https://doi.org/10.1029/2005GL023376.

Mahadevan, A., & D. Archer (2000), Modeling the impact of fronts and mesoscale circulation on the nutrient supply and biogeochemistry of the upper ocean, *Journal of Geophysical Research*, *105*, 1209–1225.

Mahadevan, A., E. D'Asaro, C. Lee, & M. J. Perry (2012), Eddy-driven stratification initiates North Atlantic spring phytoplankton blooms, *Science*, *337*, 54–58.

McGillicuddy, D. J., L. A. Anderson, S. C. Doney, & M. E. Maltrud (2003), Eddy-driven sources and sinks of nutrients in the upper ocean: Results from 0.1° resolution model of the North Atlantic, *Global Biogeochemical Cycles*, *17*, 1035.

McWilliams, J. C., F. Colas, & M. J. Molemaker (2009), Cold filamentary intensification and oceanic surface convergence lines, *Geophysical Research Letters*, *36*, https://doi.org/10.1029/2009GL039402.

Nagai, T., & S. Clayton (2017), Nutrient interleaving below the mixed layer of the Kuroshio Extension Front, *Ocean Dynamics*, *67*, 1027–1046.

Nagai, T., N. Gruber, H. Frenzel, Z. Lachkar, J. C. McWilliams, & G.-K. Plattner (2015c), Dominant role of eddies and filaments in the offshore transport of carbon and nutrients in the California Current System, *Journal of Geophysical Research*, https://doi.org/10.1002/2015JC010889.

Nagai, T., D. Hasegawa, T. Tanaka, H. Nakamura, E. Tsutsumi, R. Inoue, & T. Yamashiro (2017), First evidence of coherent bands of strong turbulent layers associated with high-wavenumber internal-wave shear in the upstream Kuroshio, *Scientific Reports*, *7*, Article 14555, https://doi.org/10.1038/s41598-017-15167-1.

Nagai, T., R. Inoue, A. Tandon, & H. Yamazaki (2015b), Evidence of enhanced double-diffusive convection below the main stream of the Kuroshio Extension, *Journal of Geophysical Research*, *120*, 8402–8421, https://doi.org/10.1002/2015JC011288.

Nagai, T., A. Tandon, E. Kunze, & A. Mahadevan (2015a), Spontaneous generation of near-inertial waves by the Kuroshio Front, *Journal of Physical Oceanography*, *45*, 2381–2406, https://doi.org/10.1175/jpo-d-14-0086.1.

Nagai, T., A. Tandon, H. Yamazaki, & M. J. Doubell (2009), Evidence of enhanced turbulent dissipation in the frontogenetic Kuroshio Front thermocline, *Geophysical Research Letters*, *36*, L12,609, https://doi.org/10.1029/2009GL038832.

Nagai, T., A. Tandon, H. Yamazaki, M. J. Doubell, & S. Gallager (2012), Direct observations of microscale turbulence and thermohaline structure in the Kuroshio Front, *Journal of Geophysical Research*, *117*, C08,013, https://doi.org/10.1029/2011JC00722.

Nakamura, H., A. Nishina, Z. Liu, F. Tanaka, M. Wimbush, & J.-H. Park (2013), Intermediate and deep water formation in the Okinawa Trough, *Journal of Geophysical Research*, *118*, 6881–6893.

Nan, F., H. Xue, F. Yu (2015), Kuroshio intrusion into the South China Sea: A review, *Progress in Oceanography*, *137*, 314–333, https://doi.org/10.1016/j.pocean.2014.05.012.

NECP (National Centers for Environmental Prediction)/National Weather Service/NOAA/U.S. Department of Commerce (2015), Observations and gridded forcing products input into the NCEP Climate Forecast System Reanalysis, https://doi.org/10.5065/D6HM56HW, last accessed 6 February 2019.

Nikurashin, M., & R. Ferrari (2011), Global energy conversion rate from geostrophic flows into internal lee waves in the deep ocean, *Geophysical Research Letters*, *38*, L08,610.

Omand, M. M., E. D'Asaro, C. Lee, M. J. Perry, N. Briggs, I. Cetini´c, & A. Mahadevan (2015), Eddy-driven subduction exports particulate organic carbon from the spring bloom, *Science*, *348*, 222–225, https://doi.org/10.1126/science.1260062.

Osborn, T. R., & C. S. Cox (1972), Oceanic fine structure, *Geophysical Fluid Dynamics*, *3*, 321–345.

Oschlies, A. (2002), Can eddies make ocean deserts bloom?, *Global Biogeochemical Cycles*, *16*(4), https://doi.org/10.1029/2001GB001830.

Oschlies, A., H. Dietze, & P. Kahler (2003), Salt-finger driven enhancement of upper ocean nutrient supply, *Geophysical Research Letters*, *30*(23), https://doi.org/10.1029/2003GL018552.

Pelegrí, J. L., & G. T. Csanady (1991), Nutrient transport and mixing in the Gulf Stream, *Journal of Geophysical Research*, *96*, 2577–2583.

Pelegrí, J. L., G. T. Csanady, & A. Martins (1996), The North Atlantic nutrient stream, *Journal of Oceanography*, *52*, 275–299.

Plougonven, R., & C. Snyder (2005), Gravity waves excited by jets: Propagation versus generation, *Geophysical Research Letters*, *32*, https://doi.org/10.1029/2005GL023730.

Plougonven, R., & C. Snyder (2007), Inertia-gravity waves spontaneously generated by jets and fronts. Part I: Different baroclinic life cycles, *Journal of the Atmospheric Sciences*, *64*, 2502–2520.

Rainville, L., & R. Pinkel (2004), Observations of energetic high-wavenumber internal waves in the Kuroshio, *Journal of Physical Oceanography*, *34*, 1495–1505.

Qiu, B., S. Chen, & G. S. Carter (2012), Time-varying parametric subharmonic instability from repeat CTD surveys in the northwestern Pacific Ocean, *Journal of Geophysical Research*, *117*, C09012, https://doi.org/10.1029/2012JC007882.

Rhines, P. B., & W. R. Young (1982), Homogenization of potential vorticity in planetary gyres, *J. Fluid Mech.*, *122*, 347–367.

Shakespeare, C. J., & A. M. Hogg (2017), Spontaneous surface generation and interior amplification of internal waves in a regional-scale ocean model, *Journal of Physical Oceanography*, *47*(4), 811–826, https://doi.org/10.1175/JPO-D-16-0188.1.

Shakespeare, C. J., & J. R. Taylor (2014), The spontaneous generation of inertia-gravity waves during frontogenesis forced by large strain: theory, *Journal of Fluid Mechanics*, *757*, 817–853.

Schmitt, R. W. (1990), On the density ratio balance in the Central Water, *Journal of Physical Oceanography*, *20*, 900–906.

Snyder, C., W. C. Skamarock, & R. Rotunno (1993), Frontal dynamics near and following frontal collapse, *Journal of the Atmospheric Sciences*, *50*, 3194–3212.

Thomas, L. N., & C. M. Lee (2005), Intensification of ocean fronts by down-front winds, *Journal of Physical Oceanography*, *35*, 1086–1102.

Tsutsumi, E., T. Matsuno, R.-C. Lien, H. Nakamura, T. Senjyu, & X. Guo (2017), Turbulent mixing within the Kuroshio in the Tokara Strait, *Journal of Geophysical Research*, *122*(9), https://doi.org/10.1002/2017JC013049.

Uchiyama, Y., Y. Suzue, & H. Yamazaki (2017), Eddy-driven nutrient transport and associated upper-ocean primary production along the Kuroshio, *Journal of Geophysical Research Oceans*, *122*, 5046–5062, https://doi.org/10.1002/2017JC012847.

Whitt, D., & L. Thomas (2013), Near inertial waves in strongly baroclinic currents. *Journal of Physical Oceanography*, *43*, 706–725, https://doi.org/10.1175/JPO-D-12-0132.1.

Whitt, D., L. Thomas, J. M., Klymak, C. M. Lee, E. A. D'Asaro (2018), Interaction of superinertial waves with submesoscale cyclonic filaments in the North Wall of the Gulf Stream, *Journal of Physical Oceanography*, *48*, 81–99.

Williams, R. G., E. McDonagh, V. M. Roussenov, S. Torres-Valdes, B. King, R. Sanders, & D. A. Hansell (2011), Nutrient streams in the North Atlantic: Advective pathways of inorganic and dissolved organic nutrients, *Global Biogeochemical Cycles*, *25*, GB4008, https://doi.org/10.1029/2010GB003853.

Williams, R. G., V. Roussenov, & M. Follows (2006), Induction of nutrients into the mixed layer and maintenance of high latitude productivity, *Global Biogeochemical Cycles*, *20*, GB1016, https://doi.org/10.1029/2005GB002586.

Wolfram, P. J., T. D. Ringler, M. E. Maltrud, D. W. Jacobsen, & M. R. Petersen (2015), Diagnosing isopycnal diffusivity in an eddying, idealized midlatitude ocean basin via Lagrangian, in situ, Global, High-Performance Particle Tracking (LIGHT), *Journal of Physical Oceanography*, *45*, 2114–2133.

Yasuda, I. (1995), Geostrophic vortex merger and streamer development in the ocean with special reference to the merger of Kuroshio warm core rings, *Journal of Physical Oceanography*, *25*, 979–996.